Microelectronic Engineering 263 (2022) 111856

Contents lists available at ScienceDirect

Microelectronic Engineering

journal homepage: www.elsevier.com/locate/mee

Controlling surface effects in extremely high aspect ratio gold plasmonic electrodes

Marco Riccardi, Christian Santschi, Olivier J.F. Martin *

Nanophotonics and Metrology Laboratory, Swiss Federal Institute of Technology Lausanne (EPFL), EPFL-STI-NAM, Station 11, CH-1015 Lausanne, Switzerland

ARTICLE INFO

Keywords:
Plasmonics
Surface forces
Adhesion layers
Self-assembled monolayers

ABSTRACT

Nanofabrication is key to many technological advances, especially the challenge of merging nanophotonics with electronics. Here, we investigate the fabrication process of plasmonic interdigitated gold electrodes having a very high aspect ratio (i.e. long and thin geometries) and a large surface area. Stringent stability issues that arise when these structures are fabricated using inorganic adhesion layers, such as titanium or chromium, on silica substrates are highlighted. We ascribe these problems to thermodynamical non-equilibrium states of freshly deposited gold and, in particular, discuss the role of surface energy in determining the structural properties of high aspect ratio gold nanostructures. We then show that the use of organic silane self-assembled monolayers improves the long term stability of these structures and, finally, characterize the fabricated electrodes. This technology can unleash the potential of hybrid optoelectronic circuits where current and light are manipulated with the same component.

1. Introduction

The continuous evolution of nanofabrication techniques in the past decades has enabled the controlled fabrication of devices with sub-100 nm features, allowing the investigation and control of physical phenomena at the quantum level and the nanoscale [1]. Arguably, the field that has benefited most from this miniaturization trend is electronics, where the number of electronic components on a single chip has steadily increased over the years [2], as anticipated by Moore. Consequently, longer and narrower interconnections are now required to join different active components located on the same substrate [3–5], and to interface these devices with the macroscopic world. Combining long and narrow intrinsically goes along with increasing the surface to volume ratio of the nanoscale structures [6,7] and makes properties such as interfacial adhesion, surface energy and diffusion of key importance. Parallel to this, there is an ongoing trend to integrate electronic and photonic capabilities into a single component that would outperform conventional semiconductor devices [8–10]. In particular, plasmonic electrodes are set to become a key component of future optoelectronic circuits thanks to their ability to both carry electronic signals and manipulate optical radiation [11]. The mutual coupling between the constituents of these complex systems gives rise to unexpected optical properties [12,13], offering compelling platforms for signal processing [10,14–16], biosensing [17,18] and hot-electron chemistry [19,20], to name a few examples. In this context, reliable fabrication strategies of high aspect ratio metallic nanowires are in strong demand. Among other metals, gold (Au) has found wide reaching applications in both electronics and plasmonics thanks to its high electrical conductivity and chemical stability, together with the ability to generate a plasmonic response in the visible and near infrared range [21–24]. Unfortunately, the fabrication of elongated gold nanostructures having extremely high surface to volume aspect ratios is a challenging task. On gold, surface self-diffusion occurs even at room temperature and, as a consequence, a gold nanostructure tends to spontaneously change its shape towards configurations with lower free energy and, hence, with a smaller surface [25–27]. In particular, freshly deposited gold thin films are especially unstable since they are in a partially amorphous phase [28,29]. This state, combined with a large surface and, hence, a high surface energy, is thermodynamically unfavorable, which further enhances surface diffusion. In addition, when working with gold films deposited on silica substrates, one has to also consider the adhesion between these two materials [30], which is neither mediated by strong chemical binding – since gold oxide is very unstable – nor by diffusion – as bulk diffusion is relatively low at room temperature [31]. Formally, good adhesion implies

$$\gamma_{s/Au} + \gamma_{Au/v} < \gamma_{s/v}, \tag{1}$$

* Corresponding author.
E-mail address: olivier.martin@epfl.ch (O.J.F. Martin).

https://doi.org/10.1016/j.mee.2022.111856
Received 31 May 2022; Received in revised form 26 July 2022; Accepted 29 July 2022
Available online 3 August 2022

where $\gamma_{s/Au}$ is the interfacial energy of the substrate / gold interface, while $\gamma_{s/v}$ and $\gamma_{Au/v}$ are, respectively, the surface energies of the substrate and the metal towards vacuum [32,33]. Clearly, an increase in $\gamma_{s/v}$ through the deposition of an adhesion layer favors the wetting of the substrate by the gold. Traditionally, good adhesion can be achieved by introducing a layer of titanium (Ti) or chromium (Cr) between the gold and the silica, leading to a thermodynamically downhill reaction with negative enthalpy of formation [34]. Higher $\gamma_{s/v}$ are generally achieved with more compact adhesion layers, supporting the common belief that thicker layers result in an enhanced adhesion between two materials due to a denser surface coverage. Interestingly, this conclusion has been challenged recently, where the diffusion of adhesion layer material into the gold layer has been shown to deteriorate its structural properties and its adhesion to the substrate [35,36]. With an eye on applications, one also has to consider that, regardless of their thickness, metallic adhesion layers have detrimental effects on the optoelectronics properties of metallic nanostructures, generally leading to an increase of their electric resistance and, consequently, to a widening and redshift of their plasmonic resonances [35–42]. The use of metallic adhesion layers is therefore not ideal for the fabrication of plasmonic structures with superior optoelectronic properties. On the other hand, different authors have reported the facile integration of molecular self-assembled monolayers (SAMs) into top-down techniques for the creation of organic adhesion layers [43–46] and, interestingly, their inkjet printing [47,48] and patterning [49–52]. Thanks to its molecular thickness, a SAM induces only a slight redshift of the plasmonic resonances, while the gold is anchored to the substrate through a series of covalent bonds that provide a strong adhesion. To this end, the ability of a thiolated substrate to spontaneously form covalent bonds with gold greatly decreases $\gamma_{s/Au}$ and leads to a better wetting than when employing metallic adhesion layers. As a consequence, organic adhesion layers support gold films with exceptional structural and optical properties [53–56] and represent promising alternatives to the use of metallic adhesion layers.

In this work, we fabricate plasmonic interdigitated gold electrodes with extremely high aspect ratios on silica substrates and explore, both experimentally and through the development of an empirical model, the influence of different inorganic and organic adhesion layers on their long term stability. First, we unveil the thermodynamic instability of freshly deposited gold nanostructures. Second, we stabilize them by using inorganic adhesion layers and subsequently demonstrate the benefits of employing organic layers to counteract the adverse action of surface forces. In particular, we will show how these high aspect ratio gold nanostructures can only be successfully fabricated with the use of organic adhesion layers. This is different from the case of low aspect ratio nanostructures where, thanks to a lower surface area, surface effects are minimized to the point that these structures can be readily fabricated with either organic or thin inorganic adhesion layers [44]. Finally, we demonstrate the utilization of such plasmonic electrodes for spectroscopic and electronic experiments and compare their experimental response with numerical calculations, before putting forth a semi-quantitative model that readily explains our experimental results in terms of change in the surface energies of our system.

2. Materials and methods

Let us describe the fabrication process of plasmonic circular gold dimers with long interconnections arranged into an interdigitated electrode array, as shown in Fig. 1. Each finger has an average aspect ratio (length/width) exceeding 220, while the whole structure possesses a surface to volume ratio greater than 40 μm^{-1}, as can be readily calculated by considering the dimensions of the large contact gold stripes. The electrodes are fabricated following the electron-beam lithography process outlined in Fig. 2. Briefly, 4-in. fused silica wafers (Schott AG, 525 μm thick) are first dried under a constant nitrogen flow for more than one week before being further dehydrated through a thermal treatment on a hotplate at 180 °C for 5 min, in order to promote resist adhesion [57]. Subsequently, 120 nm of MMA EL6 (Micro-resist Technology GmbH) are spin-coated (ATMsse OPTIspin SB20 manual coater, 6000 rpm) on the wafer, followed by 60 nm of PMMA 495K A2 (Micro-resist Technology GmbH, spin-coated at 1500 rpm). This way, the substrate is covered with a double layer of electron beam resist, which helps promoting the lift-off thanks to the formation of an undercut at the edges of the exposed areas after the development [58]. To avoid charging issues during the electron-beam exposure, a 20 nm conducting sacrificial layer of Cr is further evaporated on the resist (Alliance-Concept EVA760) and removed in a $(NH_4)_2Ce(NO_3)_6 + HClO_4$ solution (TechniEtch Cr01 from MicroChemicals) after the exposure. This is carried out with a Raith EBPG5000+ system at a 100 kV acceleration voltage, with varying beam doses between 500 and 1000 $\mu C/cm^2$ and beam currents ranging from 200 pA to 100 nA. After the Cr removal, the resist is developed in a MiBK:IPA 1:3 developer solution during 1 min under continuous circular agitation, rinsed for 1 min with isopropyl alcohol (IPA) and dried with a nitrogen gun. To fabricate the electrodes using inorganic adhesion layers, an 8 s. oxygen plasma treatment is applied to remove the residuals of undeveloped resist (Oxford PRS900, 300 sccm, 2 Torr, 500 W RF power) and to activate the surface for an improved adhesion. The same machine (Leybold Optics LAB600H) is then used to evaporate both the Ti or Cr adhesion layer and the gold film (thickness: 40 nm, deposition rate: 0.5 Å/s), without breaking the vacuum between the consecutive evaporations. For an organic adhesion layer, after developing the resist the substrate is first exposed to an oxygen plasma (Oxford PRS900, 300 sccm, 2 Torr, 500 W RF power) for 40 s. This longer plasma treatment, compared to the one used for inorganic adhesion layers, ensures both the removal of undeveloped resist and the creation of hydroxyl groups, needed for a proper silanisation, on the silica areas of interest. The sample is then readily placed for 10 h into a vacuum desiccator together with a vial containing (3-Mercaptopropyl)

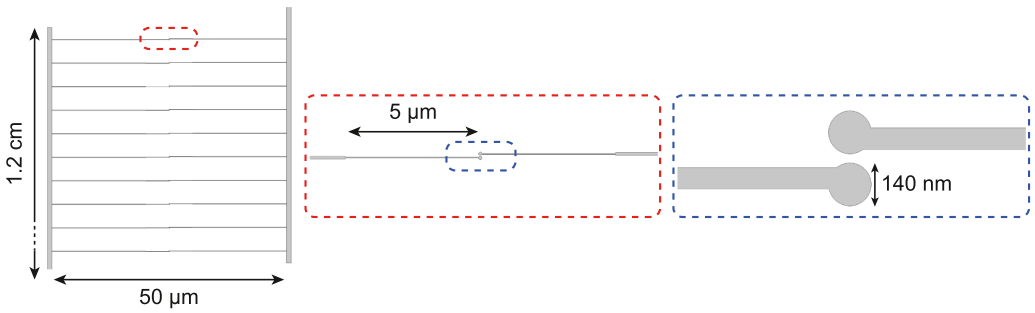

Fig. 1. Sketch of the design under study. On the left, the full interdigitated geometry is shown, where the fingers of the gold electrodes are seen extending from larger contact gold stripes (1 μm × 1.2 cm) that allow for external electrical connection. The distance between adjacent fingers is 5 m. The central panel shows a magnified view of one electrode pair and shows how each finger is composed of two connected successive sections (first 150 nm wide × 20 μm long followed by 70 nm wide × 5 μm long). At their extremity, these are joined to a 140 nm diameter disk, as displayed in the rightmost panel. The gap between two adjacent disks is 30 nm. (For interpretation of the references to colour in this figure legend, the reader is referred to the web version of this article.)

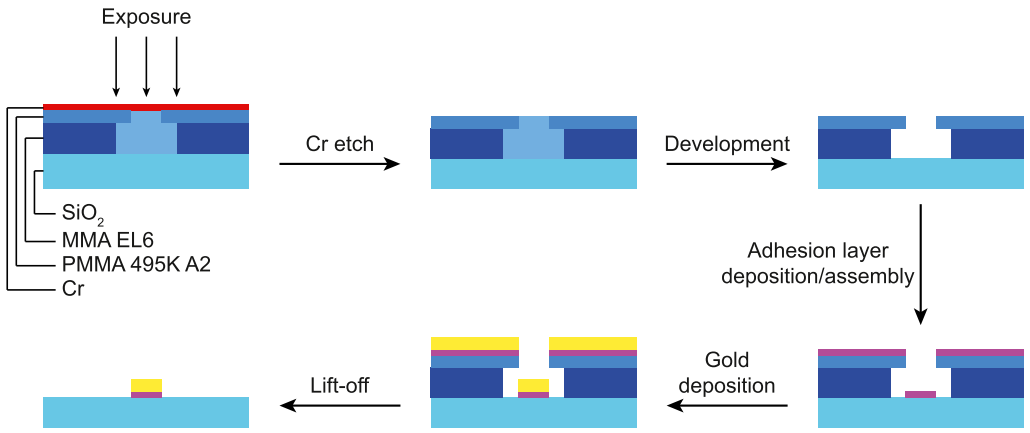

Fig. 2. Process flow for the fabrication of the structures.

trimethoxysilane (MPTMS, 95%, from Merck, used as received). The released MPTMS molecules, shown in Fig. 3(a), adsorbe on the sample, where the silane groups of the molecules establish weak hydrogen bonds with the hydroxyl groups present on the available glass surface. To stabilize the silane-glass bond, the sample is subsequently baked for 20 h at 80 °C, allowing the MPTMS to form siloxane bridges with the substrate and cross-link with adjacent molecules. The temperature is kept at 80 °C in order to prevent the destruction of the nanostructures shaped in MMA/PMMA, which has a glass temperature of about 110 °C [59,60]. Afterwards, 40 nm of gold are evaporated on the sample (Leybold Optics LAB600H, deposition rate: 0.5 Å/s), where the metal atoms covalently bind to the available thiol groups of the SAM as shown in Fig. 3(b). After the gold film deposition, an extra stabilizing baking step is performed at 80 °C for 24 h. Finally, regardless of the type of adhesion layer used, the resist is stripped by immersing the sample into an acetone bath for 24 h. Prior to the SEM characterization (ZEISS Merlin), 1.5 nm of Cr are sputtered (Alliance-Concept DP650) onto the sample to avoid charging during imaging.

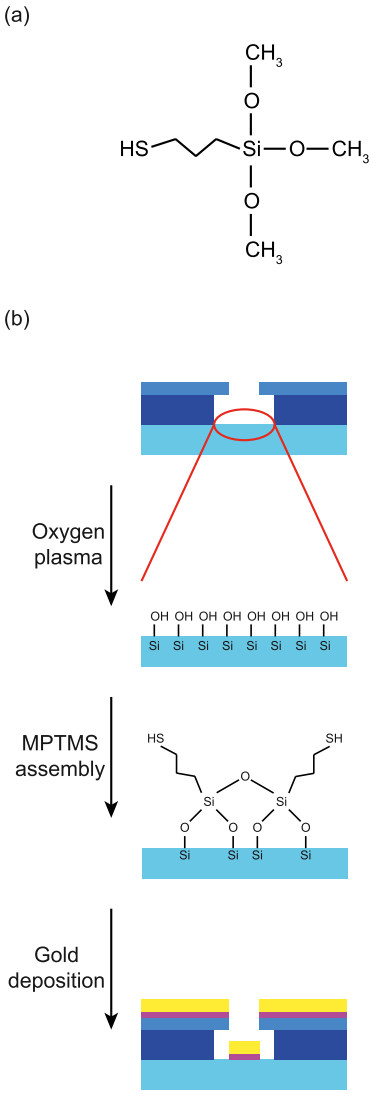

Fig. 3. (a) Structural formula of a MPTMS molecule. (b) Process flow for the realization of a surface functionalization to enhance gold adhesion with a SAM. (For interpretation of the references to colour in this figure legend, the reader is referred to the web version of this article.)

The optical characterization of the plasmonic electrodes is carried out on an Olympus IX73 inverted microscope setup. Briefly, with the help of a custom-made dark-field condenser, the white light from a halogen lamp is focused on the sample and a 60×/0.7 Olympus LUCPlanFLN objective is used to collect the forward scattered light. This is normalized with respect to the spectrum of the lamp and analyzed with the help of an Andor Kymera 328i-A spectrograph equipped with a Newton 920 CCD detector purchased from Andor. The electrical characterization is carried out on a commercial probe station from Cascade Microtech, while the data is analyzed with a Keithley 4200A-SCS parameter analyzer. These measurements were taken in air atmosphere at room temperature. To ease the characterization of the electrodes, after the lift-off a 2.5 μm protective layer of photoresist (AZ 1512 HS) is spincoated (1000 rpm, followed by a 2 min baking at 107 °C) on the wafers before these are diced into chips using a Disco DAD321 automatic dicing saw machine (25,000 rpm, cutting speed of 1 mm/s). The resist is then stripped with acetone and IPA right before the measurements are performed.

3. Results and discussion

Let us now delve with more detail into the fabrication process of plasmonic gold electrodes on silica substrates employing inorganic and organic adhesion layers, before describing a semi quantitative model that fully explains our experimental observations.

3.1. Inorganic adhesion layers and surface effects

At first we discuss the configuration with a 3 nm Ti adhesion layer. Fig. 4(a) displays the SEM images of the fabricated structures recorded within 30 min after the lift-off step and demonstrate a successful

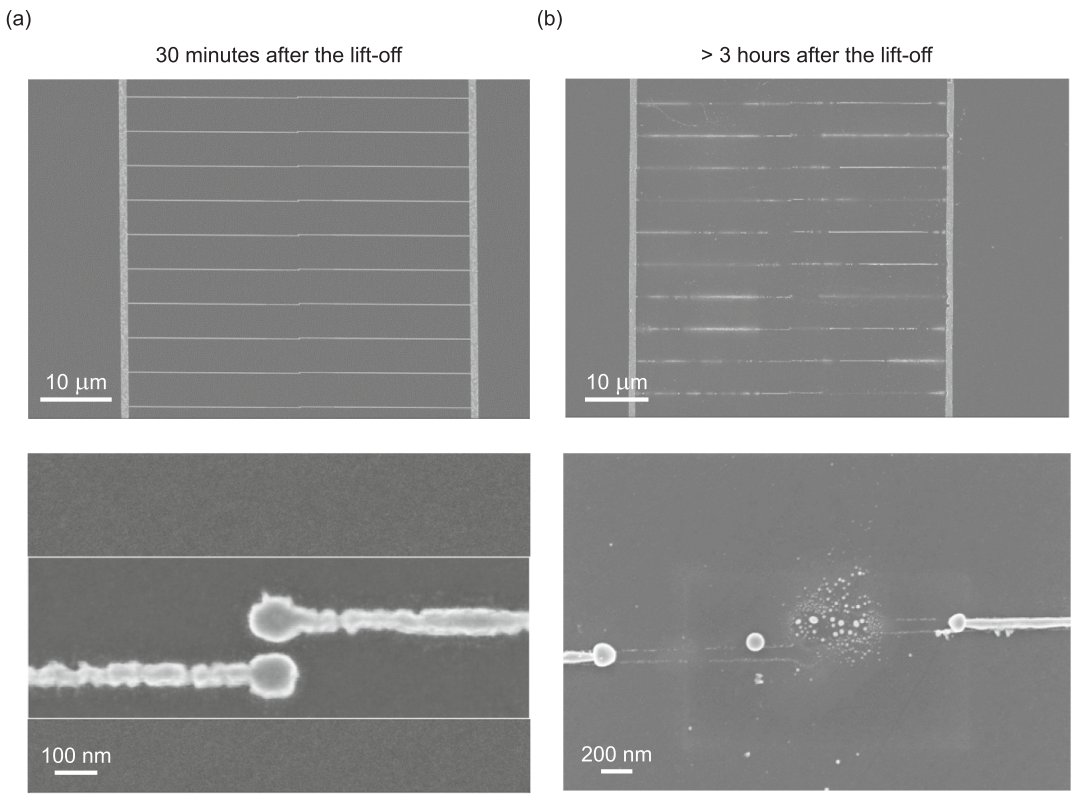

Fig. 4. SEM images of the interdigitated electrodes, with an underlying 3 nm Ti layer, recorded (a) 30 min after the lift-off and (b) more than three hours later.

fabrication of both the plasmonic disks and the long connecting rods, albeit with a significant roughness for the latter. Interestingly however, after the sample is stored for more than three hours under cleanroom conditions, one can see from Fig. 4(b) that most of the fabricated structures are destroyed. In particular, the gold diffuses over the silica surface and reorganizes into spherical aggregates. To this regard, the diffusion of gold on a glass substrate is not surprising, as the small enthalpy of formation of gold oxide hampers the creation of a stable metal-oxide interface and prevents proper wetting of the silica by the metal [34]. As a consequence, surface diffusion sets in and the gold accumulates in spherical particles, since such a shape provides the lowest surface energy for a given volume [25,34,61]. However, the ability of gold to diffuse despite the underlying Ti adhesion layer is surprising since, as we show in the Supporting Information with the help of contact angle measurements, Ti locally increases the substrate surface energy promoting wetting of gold and counteracting surface diffusion. The gold is further anchored to the substrate likely thanks to the establishment of Ti—Au bonds [62,63]. In this configuration, the gold is usually tightly anchored to the glass substrate and can even be exposed to a variety of different gaseous and liquid environments without altering its shape [64–66]. Obviously, this thermodynamic stability breaks down for configurations having adversely high surface energies and high aspect ratios such as the one reported here. Similar behaviours have been observed for heated low aspect ratio gold nanorods, which change shape and transition to a sphere in a surface-driven reorganization process [29,67–71]. However, we can safely exclude the presence of any thermal effect in our system, as all the samples are stored at room temperature. On the other hand, comparing with two other commonly used plasmonic metals such as silver and aluminum, we see that they both require specific fabrication processes when deposited onto silica [33,57]. The case of silver is particularly interesting in this context, as it belongs to the same group as gold in the periodic table and, therefore, shares with it some common chemical properties such as a low adhesion energy on glass, which manifests itself in an enhanced surface diffusion already at room temperature [33,34,57]. We hypothesize that standard thin inorganic adhesion layers provide enough surface energy to properly stabilize gold nanostructures having low aspect ratios. On the other hand, structures with larger aspect ratios possess extensive surface areas, resulting in higher surface energies. These configurations, such as the one reported here, can become thermodynamically unstable up to the point where surface effects begin to dominate their stability [72] and surface diffusion sets in. When this happens, the system evolves towards a more favourable thermodynamic state with a smaller surface area, as can be noticed when comparing Fig. 4(a) with Fig. 4(b). In this case, similarly to what happens with low aspect ratio silver structures [33], improved adhesion layers can prevent the detrimental surface diffusion of gold, revealing how the controlled modification of the metal-oxide interface is a key criterion to stabilize high aspect ratio gold structures. As an additional evidence, we show in the Supporting Information that such high aspect ratio plasmonic structures can be readily fabricated using aluminum, which easily forms a stable metal-oxide interface with the glass substrate that leads to a much higher adhesion energy [34].

We therefore tested different treatments to modify the metal-oxide interface, with the objective of preserving the shape of the structures. In particular, we fabricated large area interdigitated electrodes using Ti and Cr adhesion layers of various thicknesses – namely 3 and 10 nm – as shown in Fig. 5. The structures fabricated using 3 nm adhesion layers were completely destroyed within one day after their fabrication. The better results achieved with 3 nm Cr layers, compared to 3 nm Ti layers, can be attributed to the more favourable enthalpy of formation of chromium oxide compared to that of titanium oxide, which results into a better chromium bonding to the substrate and into a higher diffusion of Cr into gold [63]. On the other hand, as we also discuss in the Supporting Information, the use of 10 nm adhesion layers greatly increases the substrate's surface energy thanks to a better coverage, resulting in a better bonding between the silica and the gold structures and in an improved long term stability. However, we show in the Supporting

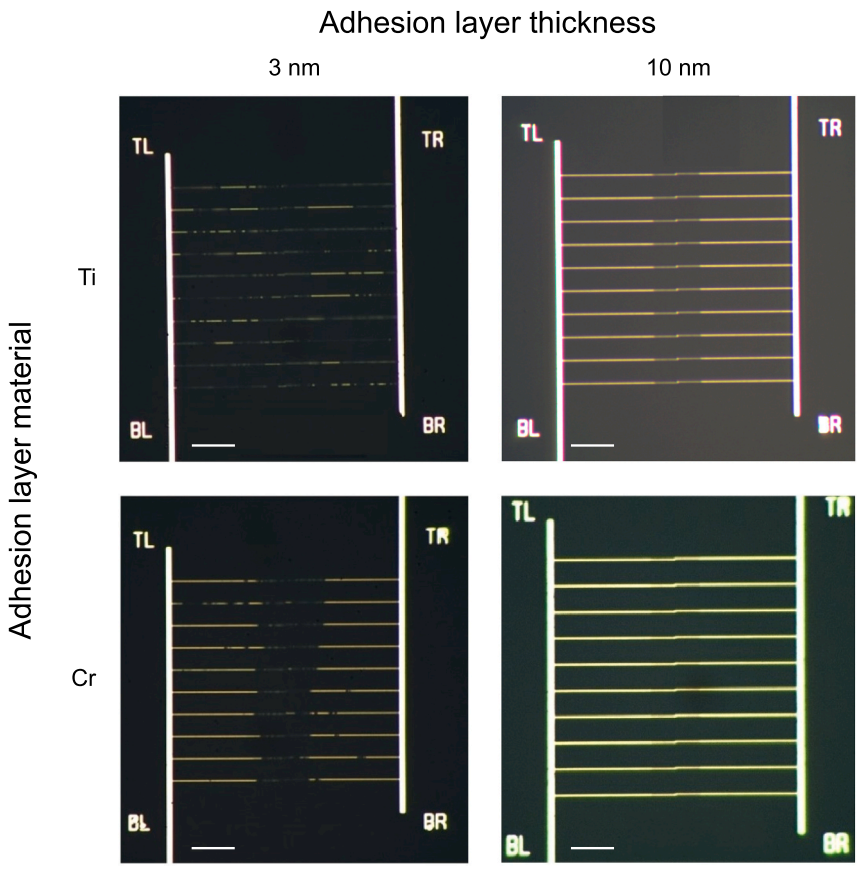

Fig. 5. Optical images of the interdigitated electrodes recorded a few days after the fabrication. Different combinations of adhesion layer materials and thicknesses are shown (10 μm scalebars).

Information that further processing of the wafers, notably dicing them into chips for optoelectronic measurements, can easily damage the electrodes, making them not suitable for practical applications. Moreover, as mentioned in the Introduction section and confirmed in the Supporting Information with the help of numerical simulations, 10 nm thick metallic adhesion layers significantly alter the plasmonic properties of the electrodes [44], notably by increasing their losses [73,74], and are therefore not suitable for the fabrication of plasmonic structures. To this end, different strategies have been proposed to minimize these harmful effects, but they all require the use of special geometries [75] or dedicated tools, such as for example cryogenic equipment [76], which are not commonly found in standard micro/nanofabrication facilities. With the idea of developing a simple and accessible fabrication process, we thus explored the use of molecular monolayers to covalently attach the gold electrodes to the silica substrate while, at the same time, keeping their optical properties unaffected.

3.2. Organosilane adhesion layer

The self-terminating deposition of molecules on a substrate, resulting in the formation of a SAM, has been a subject of study for decades now [77,78] and different techniques have been developed to produce ordered molecular layers for a variety of applications [79–82]. In particular, MPTMS has been shown to be an appropriate molecular linker between gold and silica [44,45] thanks to its thiol head group that covalently binds to gold [83,84], while the opposite methoxy groups are known to hydrolyse in the presence of water and bind to hydroxyl groups on an activated glass surface [85]. In particular, we stress the fact that the fabrication process that we propose in the Methods section allows the creation of hydroxyl groups on the exposed areas of a silica surface covered with electron-beam resist, without severely damaging the resist layer. This is a more gentle treatment when compared to standard surface activation protocols employing a Piranha solution [45,46], which can easily dissolve the PMMA layer. Once a thin layer of gold is subsequently deposited on top of a MPTMS SAM grafted onto a glass substrate, it stably binds to the available thiol groups and attaches to the underlying silica surface through a series of covalent bonds, as described in the Methods section. In the latter, we also highlighted that a post-baking step, carried out after the metal evaporation, improves the quality and stability of the nanostructures. This additional thermal treatment was found to be a crucial step in the fabrication process since freshly deposited gold is in an unstable, partially amorphous [28], state and this additional baking step stabilizes the gold structures by promoting a transition from the as-deposited unstable gold phase to a thermodynamically more stable polycrystalline morphology. To this end we note that similar structures, albeit of lower aspect ratio, have been successfully fabricated in monocrystalline gold [16,86,87], hinting at the importance of the structural properties of the metal for its stability. The chosen temperature of 80 °C is sufficient to stimulate a reorganization of the deposited gold, while preventing the destruction of the MMA/PMMA structures and the thermal desorption of the S atoms on gold, which occurs above 100 °C [83]. With an eye on optical applications, this sets a constraint on the maximum optical power that the conjugated thiol-gold system can absorb, and power densities above 1.6 mW/μm^2 in an air environment, or 11 mW/μm^2 in water, are therefore to be avoided [88]. On the other hand, the siloxane bond is stable up until about 1000 °C [49,89,90], making the thermal desorption of the silane head group from the silica substrate unlikely. However, at temperatures above 500 °C the hydrocarbon chains begin to decompose into gaseous carbon oxides, leading to the destruction of the SAM [49,89–91]. In light of all this, optical characterization of the electrodes with continuous wave light sources having power densities in the μW/

μm^2 regime carries no damage to the SAM.

Fig. 6(a) shows the nanoelectrodes fabricated with organic adhesion layers. One can notice that the fabricated structures have an excellent shape, close to the reference geometry, with remarkably smooth boundaries compared to those manufactured with inorganic adhesion layers shown in Fig. 4(a). We note that the SEM images provided here were recorded more than a week after the lift-off process, which confirms how organic MPTMS adhesion layers dramatically reduce surface diffusion and improve the long term stability of the plasmonic electrodes. Further SEM and optical characterization has also shown that the structures remain stable up to 6 months after fabrication and can survive the dicing process, allowing their experimental characterization. To this end we provide, in Fig. 6(b), the measured optical and electronic responses of the plasmonic electrodes. In particular, the left panel of Fig. 6 (b) shows the measured dark-field scattering spectrum of a single disk dimer in a water environment ($n = 1.33$). This clearly reveals a plasmonic dipole resonance at a wavelength around 1000 nm, which is in good agreement with the simulated response calculated with COMSOL Multiphysics 5.6. In the right panel, the current-voltage (IV) characteristics of the electrodes is provided, which shows a typical resistance-like behaviour. The linear fit of these data demonstrates an excellent electrical insulation between the disks, with an open-circuit resistance of 567 GΩ that allows the creation of electric fields with strengths up to $1.66 \cdot 10^8$ V/m. These results perspicuously demonstrate the possibility to fabricate plasmonic nanostructures, connected to interdigitated electrodes, with very good optoelectronic properties, paving the way for the experimental study of more exotic nanophotonic and nanoelectronic processes [13]. However, we found it challenging to fabricate smaller plasmonic structures with resonances in the visible range, even when employing very small (< 500 $\mu C/cm^2$) electron beam doses. This limitation presumably stems from the relatively long oxygen plasma treatment used to activate the silica substrate before grafting the SAM, which is likely to slightly etch the MMA/PMMA bilayer and enlarge the apertures in the resist mask. All in all, the procedure described here results in a reliable fabrication process having a yield exceeding 90%, enabling routine production and long term stability of the written structures. However, the additional baking induced some difficulties in completely lifting off the large areas between the electrodes, decreasing the electrical insulation between them. This is likely due to the removal of residual solvents during the additional baking steps, altering the resist layers towards a more compact configuration. To this end, the creation of additional sacrificial apertures in the mask was found to significantly improve the detachment of the resist.

3.3. Empirical model

After showing the beneficial effects of thiolated organic layers to stabilize high aspect ratio gold nanostructures, we describe here an

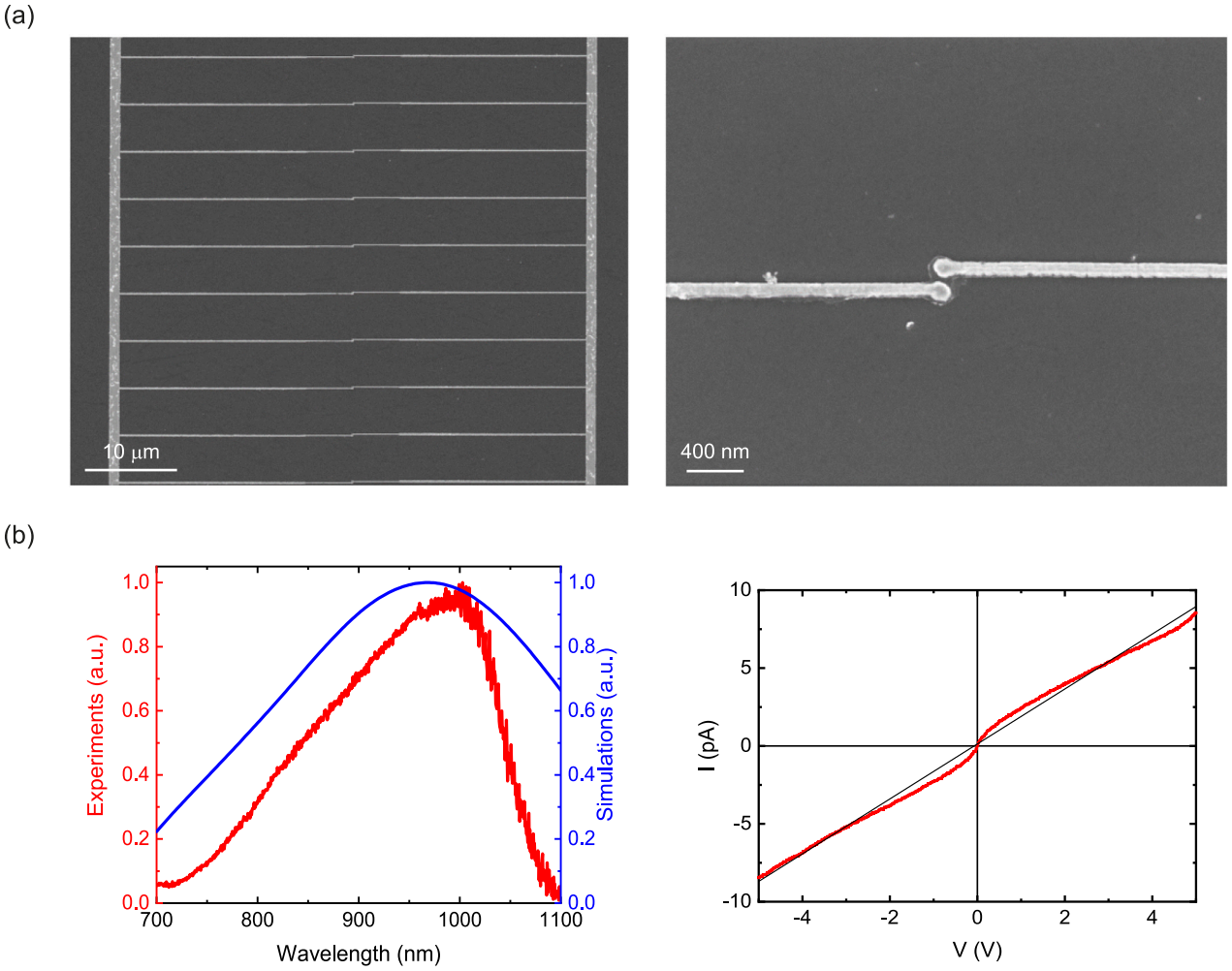

Fig. 6. (a) SEM images of the fabricated structures taken two weeks after the end of the fabrication process. (b) On the left, the normalized experimental dark-field scattering spectrum for a single plasmonic disk dimer (red) is compared to the theoretical prediction (blue). On the right, the IV characteristics of the electrodes is shown (red), together with its linear fit (black). (For interpretation of the references to colour in this figure legend, the reader is referred to the web version of this article.)

empirical model that shines light into the role that surface energies play in these structures, and explains how different adhesion layers can affect the thermodynamic equilibrium of the system. Let us refer to Fig. 7, where a schematic of the mechanism leading to the destruction of the plasmonic electrodes is proposed. In particular, we can see that this process can be ideally split into two different steps. The first is shown on top and describes the reorganization of the gold film towards a more favourable configuration with reduced surface area, all while keeping the surface between the substrate and the vacuum $A_{s/v}$ unchanged. The second mechanism, shown at the bottom of the figure, is a dewetting of the substrate by the gold film that occurs while maintaining the contact area between the gold and the vacuum $A_{Au/v}$ constant. We stress the fact that the system concurrently explores both these pathways as it relaxes from the initial configuration, where the gold is arranged in high surface area structures, to the final one, where the metal forms spherical aggregates on the substrate. A spontaneous evolution from the former to the latter case, i.e. a spontaneous destruction of the electrodes, occurs if the energy of the final configuration is lower than that of the initial one, that is if.

$$\begin{aligned} dE &= \left.\frac{dE}{dA_{Au/v}}\right|_{A_{s/v}=const.} \cdot dA_{Au/v} + \left.\frac{dE}{dA_{s/v}}\right|_{A_{Au/v}=const.} \cdot dA_{s/v} = \\ &= \gamma_{Au/v} \cdot dA_{Au/v} + \left(\gamma_{s/v} + \gamma_{Au/v} - \gamma_{s/Au}\right) \cdot dA_{s/v} < 0, \end{aligned} \tag{2}$$

where dE has been rewritten using the surface energies introduced in Eq. (1), shining light into the way these quantities govern the stability of our system. Let us start by analyzing the first term of this equation, which is evidently negative since $dA_{Au/v} < 0$ when the system moves from a configuration having high surface area to one possessing a lower surface. This represents the main mechanism behind the reorganization of the gold film, which is clearly driven by a preference for smaller surface areas and, hence, smaller surface energies. To this end, we can write $dA_{Au/v} = 0.5 \cdot V^{2/3}\, dk$, where $k \geq 1$ is a shape factor that characterizes the degree to which the area of a gold structure of volume V parts from its minimum value $0.5 \cdot V^{2/3}$ that is achieved when the gold takes the form of a semi sphere on the substrate. Higher k implies higher surface and thus $dk < 0$ in our system, as shown in Fig. 7, with its magnitude increasing for initial configurations of the structure having a higher surface area. This explains the higher instability of high aspect ratio systems when compared to low aspect ratio structures. If we now consider the second term, we see that this is composed of three contributions: the first takes into account the energy to build an area $dA_{s/v}$ at the substrate / vacuum surface, the second is the energy required to create a similar area at the metal / vacuum surface, while the third represents the energy required to split the initial substrate / gold interface. We see that $dA_{s/v} > 0$ and therefore this term generally counteracts the effect of the latter. This can be explained by rewriting $dA_{s/v} = -L_c\, dr$, where L_c is the length of the contact line between the gold and the substrate and $r > 0$ is its distance from the center of the structure. Clearly, when the electrodes evolve towards a spherical shape the contact line shrinks, as shown in Fig. 7, making $dr < 0$ and consequently $dA_{s/v} > 0$. As for the surface energy associated to this term, it can be easily appreciated now how the increase in $\gamma_{s/v}$ brought about by the

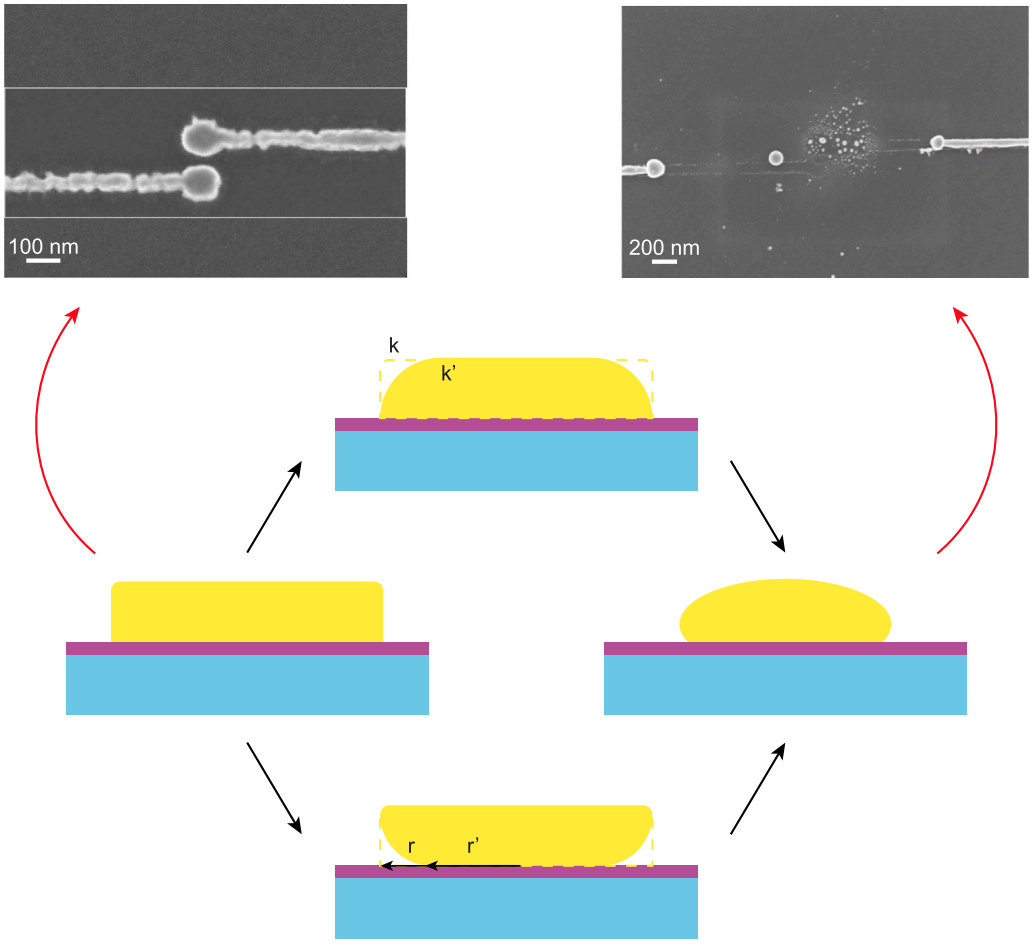

Fig. 7. Schematic of the process leading to the spontaneous destruction of the electrodes. The changes k → k' and r → r' of the parameters describing the geometry of the structure is shown for each mechanism. The bottom SEM images of Fig. 4, representing the initial and final state of the process, are also reproduced here for convenience.

deposition of a thick inorganic adhesion layer can make this term big enough to yield $dE > 0$ and completely stabilize the structures. On the other hand, we have shown in the Supporting Information that an MPTMS adhesion layer actually decreases $\gamma_{s/v}$ and does therefore not ensure proper wetting of the silica by the gold. However, when this metal is deposited on an organic layer that exposes thiol groups at its surface, these spontaneously bind to gold releasing an energy equal to the enthalpy of adsorption $\Delta H \simeq$ -80 kJ/mol of this process [92,93]. This chemical contribution to the thermodynamic stability of our system is neglected in the above discussion, but needs to be fully accounted for to thoroughly describe our structures. To this end, we can express the total interfacial energy at the thiolated substrate / gold interface as the sum of a pure surface term and a chemical term:

$$\gamma_{s/Au} = \gamma^{S}_{s/Au} + \gamma^{C}_{s/Au}, \tag{3}$$

$$\gamma^{C}_{s/Au} = \Delta H \phi, \tag{4}$$

where $\gamma^{S}_{s/Au}$ is the (positively defined) surface energy originating from the energy difference between surface and bulk molecules, while $\gamma^{C}_{s/Au}$ is the energy required to form S—Au bonds at the surface, expressed through the molar surface density of thiol groups ϕ. Clearly, $\gamma^{C}_{s/Au} < 0$ and it is therefore possible, when $|\gamma^{C}_{s/Au}| > \gamma^{S}_{s/Au}$, for the total interfacial energy $\gamma_{s/Au}$ to be negative. In such a case, the magnitude of the second term in Eq. (2) becomes larger and contributes to the lowering of the overall surface energy of the system having elongated gold structures, which is now more thermodinamically stable than that with low surface area electrodes. In practice, this situation arises only if the silica surface presents a sufficient number of thiol groups that can bind to the gold, i.e. if ϕ is high enough. Assuming a complete monolayer formation, this parameter can be estimated by referencing to Fig. 3(b), where it is shown that for every two silicon atoms on the substrate there is one corresponding thiol group at the surface. From the density ($\rho = 2.196$ g/cm^3 [94]) and molecular weight ($w = 60.08$ g/mol) of silica, one can estimate the number of molecules of silica inside a cubic centimeter of material as $N_A\rho/w$ and, therefore, their surface density as $(N_A\rho/w)^{2/3}$ – with N_A being Avogadro number. The final molar surface density of thiol groups is then simply $\phi = 0.5 \cdot (N_A\rho/w)^{2/3}/N_A = 6.52 \cdot 10^{-10}$ mol/cm^2. We can finally infer that, for the system under study, $\gamma^{C}_{s/Au}$= -52.2 μJ/cm^2 = -522 mJ/m^2. This value is about one order of magnitude greater than those of typical $\gamma_{s/Au}$ [32], and therefore explains the enhanced stability of the gold structures fabricated on thiolated adhesion layers. With an eye on Eq. (1), this higher stability stems not from an increased $\gamma_{s/v}$, as is the case for metallic adhesion layers, but rather from the formation of a stable chemical interface between the gold and the substrate, which is equivalent to decreasing $\gamma_{s/Au}$. On the other hand, this is not the case for the inorganic adhesion layers studied here, where the lower enthalpy of formation of Ti-Au and Cr-Au bonds provide a less stable binding of the gold to the substrate [95,96]. Moreover, the low surface coverage and high oxidation state of these layers greatly reduce the number of Cr or Ti atoms available to bind to the gold, i.e. ϕ, and therefore make the contribution of $\gamma^{C}_{s/Au}$ negligible in these systems.

4. Conclusions

The downscaling and merging of optical and electronic technologies often requires structures with very large surface to volume ratios. For such devices, surface effects become the dominant interaction and limit their stability and robustness. In this work, we have confirmed that these effects are especially prominent for high aspect ratio gold nanostructures and are responsible for their structural degradation shortly after their fabrication. We have demonstrated how the quality and long term stability of such structures can be improved by enhancing their adhesion to the substrate and shown the benefits of employing organic silane adhesion layers to establish strong binding forces between the metal and the underlying surface, without affecting the optical properties of the device. Furthermore, we have shown how an additional baking favors the reorganization of the gold from a freshly deposited – thermodynamically unstable – morphology towards a more stable configuration. Surface diffusion can be dramatically reduced by carrying out the baking prior to the lift-off procedure since the metal remains confined within the PMMA mold. These findings enable the fabrication of plasmonic devices with extremely high aspect ratios, which are likely to play a major role in emerging signal processing and quantum technologies since they provide a bridge to connect the nano- to the macroscales, as well as the photonic to the electronic worlds.

CRediT authorship contribution statement

Marco Riccardi: Conceptualization, Investigation, Validation, Formal analysis, Visualization, Writing – original draft. **Christian Santschi:** Resources, Methodology, Formal analysis, Writing – review & editing, Supervision. **Olivier J.F. Martin:** Conceptualization, Writing – review & editing, Supervision, Project administration, Funding acquisition.

Declaration of Competing Interest

Olivier J. F. Martin reports financial support was provided by European Research Council.

Acknowledgements

We gratefully acknowledge funding from the European Research Council (ERC-2015-AdG-695206 Nanofactory). We are thankful to Dr. Nicolò Oliva and Carlotta Gastaldi for their help with the electrical characterization of the devices.

Appendix A. Supplementary data

Supplementary data to this article can be found online at https://doi.org/10.1016/j.mee.2022.111856.

References

[1] B. Bhushan (Ed.), Springer Handbook of Nanotechnology, 4th edition, Springer, 2017.
[2] T.N. Theis, H.-S.P. Wong, The end of Moore's law: a new beginning for information technology, Comput. Sci. Eng. 19 (2) (2017) 41–50, https://doi.org/10.1109/MCSE.2017.29. URL, http://ieeexplore.ieee.org/document/7878935/.
[3] R. Havemann, J. Hutchby, High-performance interconnects: an integration overview, Proc. IEEE 89 (5) (2001) 586–601, https://doi.org/10.1109/5.929646. URL, http://ieeexplore.ieee.org/document/929646/.
[4] M. Su, Z. Huang, Y. Huang, S. Chen, X. Qian, W. Li, Y. Li, W. Pei, H. Chen, F. Li, Y. Song, Swarm intelligence-inspired spontaneous fabrication of optimal interconnect at the micro/nanoscale, Adv. Mater. 29 (7) (2017) 1605223, https://doi.org/10.1002/adma.201605223.
[5] S. Salahuddin, K. Ni, S. Datta, The era of hyper-scaling in electronics, Nat. Electron. 1 (8) (2018) 442–450, https://doi.org/10.1038/s41928-018-0117-x. URL, http://www.nature.com/articles/s41928-018-0117-x.
[6] A.V. Teplyakov, S.F. Bent, Semiconductor surface functionalization for advances in electronics, energy conversion, and dynamic systems, J. Vac. Sci. Technol. A 31 (5) (2013), 050810, https://doi.org/10.1116/1.4810784.
[7] A. Vilan, D. Cahen, Chemical modification of semiconductor surfaces for molecular electronics, Chem. Rev. 117 (5) (2017) 4624–4666, https://doi.org/10.1021/acs.chemrev.6b00746.
[8] M.L. Brongersma, V.M. Shalaev, The case for Plasmonics, Science 328 (5977) (2010) 440–441, https://doi.org/10.1126/science.1186905.
[9] T.J. Davis, D.E. Gómez, A. Roberts, Plasmonic circuits for manipulating optical information, Nanophotonics 6 (3) (2016) 543–559, https://doi.org/10.1515/nanoph-2016-0131.
[10] W. Du, T. Wang, H.-S. Chu, C.A. Nijhuis, Highly efficient on-chip direct electronic–plasmonic transducers, Nat. Photonics 11 (10) (2017) 623–627, https://doi.org/10.1038/s41566-017-0003-5. URL, http://www.nature.com/articles/s41566-017-0003-5.
[11] A. Manolis, P.J. Cegielski, L. Markey, J.-C. Weeber, A. Dereux, N. Pleros, E. Chatzianagnostou, G. Dabos, D. Ketzaki, D. Tsiokos, B. Chmielak, S. Suckow, A. L. Giesecke, C. Porschatis, Bringing Plasmonics into CMOS photonic foundries: aluminum Plasmonics on Si$_{3}$N$_{4}$ for biosensing applications,

J. Lightwave Technol. 37 (21) (2019) 5516–5524, https://doi.org/10.1109/JLT.2019.2937454. https://ieeexplore.ieee.org/document/8812760/.
[12] A. Manolis, E. Chatzianagnostou, G. Dabos, N. Pleros, B. Chmielak, A.L. Giesecke, C. Porschatis, P.J. Cegielski, L. Markey, J.-C. Weeber, A. Dereux, D. Tsiokos, Plasmonics co-integrated with silicon nitride photonics for high-sensitivity interferometric biosensing, Opt. Express 27 (12) (2019) 17102, https://doi.org/10.1364/OE.27.017102. URL, https://opg.optica.org/abstract.cfm?URI=oe-27-12-17102.
[13] M. Riccardi, O.J.F. Martin, Role of electric currents in the Fano resonances of connected plasmonic structures, Opt. Express 29 (8) (2021) 11635, https://doi.org/10.1364/OE.421951. URL, https://opg.optica.org/abstract.cfm?URI=oe-29-8-11635.
[14] J.T. Kim, J.J. Ju, S. Park, M.-S. Kim, S.K. Park, M.-H. Lee, Chip-to-chip optical interconnect using gold long-range surface plasmon polariton waveguides, Opt. Express 16 (17) (2008) 13133, https://doi.org/10.1364/OE.16.013133. https://opg.optica.org/oe/abstract.cfm?uri=oe-16-17-13133.
[15] Y. Liu, J. Zhang, H. Liu, S. Wang, L.-M. Peng, Electrically driven monolithic subwavelength plasmonic interconnect circuits, Sci. Adv. 3 (10) (2017) 1701456, https://doi.org/10.1126/sciadv.1701456.
[16] R. Kullock, M. Ochs, P. Grimm, M. Emmerling, B. Hecht, Electrically-driven Yagi-Uda antennas for light, Nat. Commun. 11 (1) (2020) 115, https://doi.org/10.1038/s41467-019-14011-6. URL, http://www.nature.com/articles/s41467-019-14011-6.
[17] M. Dipalo, G.C. Messina, H. Amin, R. La Rocca, V. Shalabaeva, A. Simi, A. Maccione, P. Zilio, L. Berdondini, F. De Angelis, 3D plasmonic nanoantennas integrated with MEA biosensors, Nanoscale 7 (8) (2015) 3703–3711.
[18] L. Hong, H. Li, H. Yang, K. Sengupta, Nano-plasmonics and electronics co-integration in CMOS enabling a pill-sized multiplexed fluorescence microarray system, Biomed. Optics Express 9 (11) (2018) 5735, https://doi.org/10.1364/BOE.9.005735. URL, https://opg.optica.org/abstract.cfm?URI=boe-9-11-5735.
[19] P. Zilio, M. Dipalo, F. Tantussi, G.C. Messina, F. de Angelis, Hot electrons in water: injection and ponderomotive acceleration by means of plasmonic nanoelectrodes, Light: Sci. Appl. 6 (6) (2017) e17002, https://doi.org/10.1038/lsa.2017.2. URL, http://www.nature.com/articles/lsa20172.
[20] R.M. Osgood, M. Kang, K.-B. Kim, Y. Ait-El-Aoud, S. Dinneen, S. Kooi, G. Fernandes, J.M. Xu, Nanorectenna spectrally-selective plasmonic hot electron response to visible-light lasers, Nanotechnology 31 (13) (2020), 135207, https://doi.org/10.1088/1361-6528/ab60c9.
[21] P. Goodman, Current and future uses of gold in electronics, Gold Bull. 35 (1) (2002) 21–26, https://doi.org/10.1007/BF03214833.
[22] G. Schmid, B. Corain, Nanoparticulated gold: syntheses, structures, electronics, and Reactivities, Eur. J. Inorg. Chem. (2003) 3081–3098, https://doi.org/10.1002/ejic.200300187. www.eurjic.org.
[23] T.W. Ellis, The future of gold in electronics, Gold Bull. 37 (1–2) (2004) 66–71.
[24] H. Chen, L. Shao, Q. Li, J. Wang, Gold nanorods and their plasmonic properties, Chem. Soc. Rev. 42 (7) (2013) 2679–2724, https://doi.org/10.1039/C2CS35367A. URL, http://xlink.rsc.org/?DOI=C2CS35367A.
[25] P. Buffat, J.-P. Borel, Size effect on the melting temperature of gold particles, Phys. Rev. A 13 (6) (1976) 2287–2298, https://doi.org/10.1103/PhysRevA.13.2287.
[26] M. Drechsler, B.L. Blackford, A.M. Putnam, M.H. Jericho, A measurement of a surface self-diffusion coefficient by scanning tunneling microscopy, Le Journal de Physique Colloques 50 (C8) (1989) 8–223, https://doi.org/10.1051/jphyscol:1989838.
[27] A. Surrey, D. Pohl, L. Schultz, B. Rellinghaus, Quantitative measurement of the surface self-diffusion on au nanoparticles by aberration-corrected transmission electron microscopy, Nano Lett. 12 (12) (2012) 6071–6077, https://doi.org/10.1021/nl302280x.
[28] M.C. Barnes, D.-Y. Kim, H.S. Ahn, C.O. Lee, N.M. Hwang, Deposition mechanism of gold by thermal evaporation: approach by charged cluster model, J. Cryst. Growth 213 (1–2) (2000) 83–92, https://doi.org/10.1016/S0022-0248(00)00359-6. URL, https://linkinghub.elsevier.com/retrieve/pii/S0022024800003596.
[29] D. Ray, H. Wang, J. Kim, C. Santschi, O.J.F. Martin, A low-temperature annealing method for alloy nanostructures and Metasurfaces: unlocking a novel degree of freedom, Adv. Mater. 34 (17) (2022) 2108225, https://doi.org/10.1002/adma.202108225.
[30] K.E. Haq, K.H. Behrndt, I. Kobin, Adhesion mechanism of gold-Underlayer film combinations to oxide substrates, J. Vac. Sci. Technol. 6 (1) (1969) 148–152, https://doi.org/10.1116/1.1492648.
[31] E. Darque-Ceretti, D. Hélary, M. Aucouturier, An investigation of gold/ceramic and gold/glass interfaces, Gold Bull. 35 (4) (2002) 118–129, https://doi.org/10.1007/BF03214853.
[32] J.N. Israelachvili, Intermolecular and Surface Forces, 3rd edition, Elsevier, 2011.
[33] K. Thyagarajan, C. Santschi, P. Langlet, O.J.F. Martin, Highly improved fabrication of ag and Al nanostructures for UV and nonlinear Plasmonics, Adv. Opt. Mater. 4 (6) (2016) 871–876, https://doi.org/10.1002/adom.201500740.
[34] C.T. Campbell, Ultrathin metal films and particles on oxide surfaces: structural, electronic and chemisorptive properties, Surf. Sci. Rep. 27 (1–3) (1997) 1–111, https://doi.org/10.1016/S0167-5729(96)00011-8. URL, https://linkinghub.elsevier.com/retrieve/pii/S0167572996000118.
[35] W.M. Abbott, C.P. Murray, C. Zhong, C. Smith, C. McGuinness, E. Rezvani, C. Downing, D. Daly, A.K. Petford-Long, F. Bello, D. McCloskey, J.F. Donegan, Less is more: improved thermal stability and Plasmonic response in au films via the use of SubNanometer Ti adhesion layers, ACS Appl. Mater. Interfaces 11 (7) (2019) 7607–7614, https://doi.org/10.1021/acsami.8b21193.
[36] W.M. Abbott, C.P. Murray, S. Ní Lochlainn, F. Bello, C. Zhong, C. Smith, E. K. McCarthy, C. Downing, D. Daly, A.K. Petford-Long, C. McGuinness, I.I. Chunin, J.F. Donegan, D. McCloskey, Comparison of metal adhesion layers for au films in thermoplasmonic applications, ACS Appl. Mater. Interfaces 12 (11) (2020) 13503–13509, https://doi.org/10.1021/acsami.9b22279.
[37] J. Kottmann, O. Martin, Influence of the cross section and the permittivity on the plasmon-resonance spectrum of silver nanowires, Appl. Phys. B Lasers Opt. 73 (4) (2001) 299–304, https://doi.org/10.1007/s003400100698.
[38] X. Jiao, J. Goeckeritz, S. Blair, M. Oldham, Localization of near-field resonances in bowtie antennae: influence of adhesion layers, Plasmonics 4 (1) (2009) 37–50, https://doi.org/10.1007/s11468-008-9075-x.
[39] H. Aouani, J. Wenger, D. Gérard, H. Rigneault, E. Devaux, T.W. Ebbesen, F. Mahdavi, T. Xu, S. Blair, Crucial role of the adhesion layer on the plasmonic fluorescence enhancement, ACS Nano 3 (7) (2009) 2043–2048, https://doi.org/10.1021/nn900460t.
[40] B. Lahiri, R. Dylewicz, R.M. De La Rue, N.P. Johnson, Impact of titanium adhesion layers on the response of arrays of metallic split-ring resonators (SRRs), Opt. Express 18 (11) (2010), 11202, https://doi.org/10.1364/OE.18.011202. URL, https://opg.optica.org/oe/abstract.cfm?uri=oe-18-11-11202.
[41] M. Najiminaini, F. Vasefi, B. Kaminska, J.J. Carson, Optical resonance transmission properties of nano-hole arrays in a gold film: effect of adhesion layer, Opt. Express 19 (27) (2011), 26186, https://doi.org/10.1364/OE.19.026186. URL, https://opg.optica.org/oe/abstract.cfm?uri=oe-19-27-26186.
[42] S.J. Madsen, M. Esfandyarpour, M.L. Brongersma, R. Sinclair, Observing Plasmon damping due to adhesion layers in gold nanostructures using Electron energy loss spectroscopy, ACS Photon. 4 (2) (2017) 268–274, https://doi.org/10.1021/acsphotonics.6b00525.
[43] G.-J. Zhang, T. Tanii, T. Zako, T. Hosaka, T. Miyake, Y. Kanari, T. Funatsu, I. Ohdomari, Nanoscale patterning of protein using electron beam lithography of organosilane self-assembled monolayers, Small 1 (8–9) (2005) 833–837, https://doi.org/10.1002/smll.200500091.
[44] T.G. Habteyes, S. Dhuey, E. Wood, D. Gargas, S. Cabrini, P.J. Schuck, A. P. Alivisatos, S.R. Leone, Metallic adhesion layer induced plasmon damping and molecular linker as a nondamping alternative, ACS Nano 6 (6) (2012) 5702–5709, https://doi.org/10.1021/nn301885u.
[45] P.K. Gothe, D. Gaur, V.G. Achanta, MPTMS self-assembled monolayer deposition for ultra-thin gold films for plasmonics, J. Phys. Commun. 2 (3) (2018), 035005, https://doi.org/10.1088/2399-6528/aaaedd.
[46] M.F. Heinig, A. Bastos da Silva Fanta, J.B. Wagner, S. Kadkhodazadeh, Aminopropylsilatrane linkers for easy and fast fabrication of high-quality 10 nm thick gold films on SiO 2 substrates, ACS Appl, Nano Mater. 3 (5) (2020) 4418–4427, https://doi.org/10.1021/acsanm.0c00531.
[47] I. Rianasari, L. Walder, M. Burchardt, I. Zawisza, G. Wittstock, Inkjet-printed thiol self-assembled monolayer structures on gold: quality control and microarray electrode fabrication, Langmuir 24 (16) (2008) 9110–9117, https://doi.org/10.1021/la800711m.
[48] C. Belgardt, E. Sowade, T. Blaudeck, T. Baumgärtel, H. Graaf, C. von Borczyskowski, R.R. Baumann, Inkjet printing as a tool for the patterned deposition of octadecylsiloxane monolayers on silicon oxide surfaces, Phys. Chem. Chem. Phys. 15 (20) (2013) 7494, https://doi.org/10.1039/c3cp50331c. URL, http://xlink.rsc.org/?DOI=c3cp50331c.
[49] T. Balgar, S. Franzka, N. Hartmann, Laser-assisted decomposition of alkylsiloxane monolayers at ambient conditions: rapid patterning below the diffraction limit, Appl. Phys. A 82 (4) (2006) 689–695, https://doi.org/10.1007/s00339-005-3439-2.
[50] N. Hartmann, T. Balgar, R. Bautista, S. Franzka, Direct laser patterning of octadecylsiloxane monolayers on surface-oxidized silicon substrates: indications for a photothermal excitation mechanism, Surf. Sci. 600 (18) (2006) 4034–4038, https://doi.org/10.1016/j.susc.2006.01.118. URL, https://linkinghub.elsevier.com/retrieve/pii/S0039602806004626.
[51] X. Zhou, F. Boey, F. Huo, L. Huang, H. Zhang, Chemically functionalized surface patterning, Small 7 (16) (2011) 2273–2289, https://doi.org/10.1002/smll.201002381.
[52] A. Schröter, M. Mathieu, S. Franzka, J. Feydt, S. Irsen, N. Hartmann, Fabrication of chemical templates via selective laser-induced desorption of hexadecanethiol self-assembled monolayers, Appl. Surf. Sci. 278 (2013) 57–61, https://doi.org/10.1016/j.apsusc.2012.12.135. URL, https://linkinghub.elsevier.com/retrieve/pii/S0169433212023008.
[53] A.K. Mahapatro, A. Scott, A. Manning, D.B. Janes, Gold surface with sub-nm roughness realized by evaporation on a molecular adhesion monolayer, Appl. Phys. Lett. 88 (15) (2006), 151917, https://doi.org/10.1063/1.2183820.
[54] L. Leandro, R. Malureanu, N. Rozlosnik, A. Lavrinenko, Ultrathin, Ultrasmooth gold layer on dielectrics without the use of additional metallic adhesion layers, ACS Appl. Mater. Interfaces 7 (10) (2015) 5797–5802, https://doi.org/10.1021/am508681u.
[55] I. Arghir, D. Spasic, B.E. Verlinden, F. Delport, J. Lammertyn, Improved surface plasmon resonance biosensing using silanized optical fibers, Sensors Actuators B Chem. 216 (2015) 518–526, https://doi.org/10.1016/j.snb.2015.04.069. URL, https://linkinghub.elsevier.com/retrieve/pii/S0925400515005213.
[56] J. Sukham, O. Takayama, A.V. Lavrinenko, R. Malureanu, High-quality ultrathin gold layers with an APTMS adhesion for optimal performance of surface plasmon polariton-based devices, ACS Appl. Mater. Interfaces 9 (29) (2017) 25049–25056, https://doi.org/10.1021/acsami.7b07181.
[57] X. Wang, C. Santschi, O.J.F.F. Martin, Strong improvement of long-term chemical and thermal stability of plasmonic silver nanoantennas and films, Small 13 (2017) 1700044, https://doi.org/10.1002/SMLL.201700044.

[58] B. Abasahl, C. Santschi, T.V. Raziman, O.J.F. Martin, Fabrication of plasmonic structures with well-controlled nanometric features: a comparison between lift-off and ion beam etching, Nanotechnology 32 (47) (2021), 475202, https://doi.org/10.1088/1361-6528/ac1a93.

[59] L. Smith, V. Schmitz, The effect of water on the glass transition temperature of poly (methyl methacrylate), Polymer 29 (10) (1988) 1871–1878, https://doi.org/10.1016/0032-3861(88)90405-3. URL, https://linkinghub.elsevier.com/retrieve/pii/0032386188904053.

[60] Y. Grohens, M. Brogly, C. Labbe, M.-O. David, J. Schultz, Glass transition of Stereoregular poly(methyl methacrylate) at interfaces, Langmuir 14 (11) (1998) 2929–2932, https://doi.org/10.1021/la971397w.

[61] R. Sangiorgi, M.L. Muolo, D. Chatain, N. Eustathopoulos, Wettability and work of adhesion of nonreactive liquid metals on silica, J. Am. Ceram. Soc. 71 (9) (1988) 742–748, https://doi.org/10.1111/j.1151-2916.1988.tb06407.x.

[62] Y. Erdogdu, T. Jian, G.V. Lopez, W.-L. Li, L.-S. Wang, On the electronic structure and chemical bonding of titanium tetraauride: TiAu 4 and TiAu 4, Chem. Phys. Lett. 610-611 (2014) 23–28, https://doi.org/10.1016/j.cplett.2014.07.018. URL, https://linkinghub.elsevier.com/retrieve/pii/S0009261414005946.

[63] M. Todeschini, A. Bastos da Silva Fanta, F. Jensen, J.B. Wagner, A. Han, Influence of Ti and Cr adhesion layers on ultrathin Au films, ACS Appl. Mater. Interfaces 9 (42) (2017) 37374–37385, https://doi.org/10.1021/acsami.7b10136.

[64] L. Huang, S.J. Maerkl, O.J.F. Martin, Integration of plasmonic trapping in a microfluidic environment, Opt. Express 17 (8) (2009) 6018, https://doi.org/10.1364/OE.17.006018. URL, https://opg.optica.org/abstract.cfm?URI=oe-17-8-6018.

[65] N. Liu, M.L. Tang, M. Hentschel, H. Giessen, A.P. Alivisatos, Nanoantenna-enhanced gas sensing in a single tailored nanofocus, Nat. Mater. 10 (8) (2011) 631–636, https://doi.org/10.1038/nmat3029. URL, https://www.nature.com/articles/nmat3029.

[66] Y. Jin, Engineering plasmonic gold nanostructures and metamaterials for biosensing and nanomedicine, Adv. Mater. 24 (2012) 5153–5165, https://doi.org/10.1002/ADMA.201200622.

[67] S. Link, Z.L. Wang, M.A. El-Sayed, How does a gold Nanorod melt? J. Phys. Chem. B 104 (33) (2000) 7867–7870, https://doi.org/10.1021/jp0011701.

[68] Y. Wang, S. Teitel, C. Dellago, Surface-driven bulk reorganization of gold Nanorods, Nano Lett. 5 (11) (2005) 2174–2178, https://doi.org/10.1021/nl051149h.

[69] H. Petrova, J. Perez Juste, I. Pastoriza-Santos, G.V. Hartland, L.M. Liz-Marzán, P. Mulvaney, On the temperature stability of gold nanorods: comparison between thermal and ultrafast laser-induced heating, Phys. Chem. Chem. Phys. 8 (7) (2006) 814–821, https://doi.org/10.1039/B514644E. URL, http://xlink.rsc.org/?DOI=B514644E.

[70] Y. Horiguchi, K. Honda, Y. Kato, N. Nakashima, Y. Niidome, Photothermal reshaping of gold nanorods depends on the passivating layers of the nanorod surfaces, Langmuir 24 (20) (2008) 12026–12031, https://doi.org/10.1021/la800811j.

[71] N.A. Joy, B.K. Janiszewski, S. Novak, T.W. Johnson, S.-H. Oh, A. Raghunathan, J. Hartley, M.A. Carpenter, Thermal stability of gold nanorods for high-temperature plasmonic sensing, J. Phys. Chem. C 117 (22) (2013) 11718–11724, https://doi.org/10.1021/jp400607s.

[72] N. Mameka, J. Markmann, J. Weissmüller, On the impact of capillarity for strength at the nanoscale, Nat. Commun. 8 (1) (2017) 1976, https://doi.org/10.1038/s41467-017-01434-2. URL, http://www.nature.com/articles/s41467-017-01434-2.

[73] B.J. Roxworthy, K.C. Toussaint, Plasmonic nanotweezers: strong influence of adhesion layer and nanostructure orientation on trapping performance, Opt. Express 20 (9) (2012) 9591, https://doi.org/10.1364/OE.20.009591. URL, https://opg.optica.org/abstract.cfm?URI=oe-20-9-9591.

[74] D.T. Debu, P.K. Ghosh, D. French, J.B. Herzog, Surface plasmon damping effects due to Ti adhesion layer in individual gold nanodisks, Opt. Mater. Express 7 (1) (2017) 73, https://doi.org/10.1364/OME.7.000073. URL, https://opg.optica.org/abstract.cfm?URI=ome-7-1-73.

[75] T. Siegfried, Y. Ekinci, O.J. Martin, H. Sigg, Engineering metal adhesion layers that do not deteriorate Plasmon resonances, ACS Nano 7 (3) (2013) 2751–2757, https://doi.org/10.1021/nn4002006.

[76] R. Lemasters, C. Zhang, M. Manjare, W. Zhu, J. Song, S. Urazhdin, H.J. Lezec, A. Agrawal, H. Harutyunyan, Ultrathin wetting layer-free plasmonic gold films, ACS Photon. 6 (11) (2019) 2600–2606, https://doi.org/10.1021/acsphotonics.9b00907.

[77] A. Ulman, Formation and structure of self-assembled monolayers, Chem. Rev. 96 (4) (1996) 1533–1554, https://doi.org/10.1021/cr9502357.

[78] P. Atkins, J. de Paula, J. Keeler, Atkins' Physical Chemistry, 11th edition, Oxford University Press, 2018.

[79] J. Sagiv, Organized monolayers by adsorption. 1. Formation and structure of oleophobic mixed monolayers on solid surfaces, J. Am. Chem. Soc. 102 (1) (1980) 92–98, https://doi.org/10.1021/ja00521a016.

[80] B.C. Bunker, R.W. Carpick, R.A. Assink, M.L. Thomas, M.G. Hankins, J.A. Voigt, D. Sipola, M.P. de Boer, G.L. Gulley, The impact of solution agglomeration on the deposition of self-assembled monolayers, Langmuir 16 (20) (2000) 7742–7751, https://doi.org/10.1021/la000502q.

[81] N.R. Glass, R. Tjeung, P. Chan, L.Y. Yeo, J.R. Friend, Organosilane deposition for microfluidic applications, Biomicrofluidics 5 (3) (2011), 036501, https://doi.org/10.1063/1.3625605.

[82] E. Caroca, T. Sandoval, Role of organic molecules in enabling modern technology, J. Vac. Sci. Technol. A 38 (4) (2020), 043201, https://doi.org/10.1116/6.0000099.

[83] C. Vericat, M.E. Vela, G. Benitez, P. Carro, R.C. Salvarezza, Self-assembled monolayers of thiols and dithiols on gold: new challenges for a well-known system, Chem. Soc. Rev. 39 (5) (2010) 1805, https://doi.org/10.1039/b907301a. URL, http://xlink.rsc.org/?DOI=b907301a.

[84] H. Häkkinen, The gold–sulfur interface at the nanoscale, Nat. Chem. 4 (6) (2012) 443–455, https://doi.org/10.1038/nchem.1352. http://www.nature.com/articles/nchem.1352.

[85] C.M. Halliwell, A.E.G. Cass, A factorial analysis of Silanization conditions for the immobilization of oligonucleotides on glass surfaces, Anal. Chem. 73 (11) (2001) 2476–2483, https://doi.org/10.1021/ac0010633.

[86] J.C. Prangsma, J. Kern, A.G. Knapp, S. Grossmann, M. Emmerling, M. Kamp, B. Hecht, Electrically connected resonant optical antennas, Nano Lett. 12 (8) (2012) 3915–3919, https://doi.org/10.1021/nl3007374.

[87] J. Kern, R. Kullock, J. Prangsma, M. Emmerling, M. Kamp, B. Hecht, Electrically driven optical antennas, Nat. Photonics 9 (9) (2015) 582–586, https://doi.org/10.1038/nphoton.2015.141. URL, http://www.nature.com/articles/nphoton.2015.141.

[88] M. Mochizuki, S. Asatyas, K. Suthiwanich, T. Hayashi, Thiol molecules as temperature sensors for surface-enhanced Raman scattering measurements of heat-sensitive materials, Chem. Lett. 45 (10) (2016) 1207–1209, https://doi.org/10.1246/cl.160572.

[89] G.J. Kluth, M.M. Sung, R. Maboudian, Thermal behavior of Alkylsiloxane self-assembled monolayers on the oxidized Si(100) surface, Langmuir 13 (14) (1997) 3775–3780, https://doi.org/10.1021/la970135r.

[90] B. Klingebiel, A. Schröter, S. Franzka, N. Hartmann, Photothermally induced bromination and decomposition of alkylsiloxane monolayers on surface-oxidized silicon substrates, J. Vac. Sci. Technol. A 28 (4) (2010) 834–837, https://doi.org/10.1116/1.3386590.

[91] S. Franzka, J. Koch, B.N. Chichkov, N. Hartmann, Nonlinear femtosecond laser processing of alkylsiloxane monolayers on surface-oxidized silicon substrates, J. Vac. Sci. Technol. A 28 (4) (2010) 814–817, https://doi.org/10.1116/1.3281296.

[92] H.M. Schessler, D.S. Karpovich, G.J. Blanchard, Quantitating the balance between Enthalpic and entropic forces in Alkanethiol/gold monolayer self assembly, J. Am. Chem. Soc. 118 (40) (1996) 9645–9651, https://doi.org/10.1021/ja961565r.

[93] V. Ravi, J.M. Binz, R.M. Rioux, Thermodynamic profiles at the solvated inorganic–organic interface: the case of gold–thiolate monolayers, Nano Lett. 13 (2013) 4442–4448, https://doi.org/10.1021/nl402315z.

[94] D.R. Lide (Ed.), CRC Handbook of Chemistry and Physics - Internet Version, CRC Press, 2005.

[95] F.R. de Boer, R. Boom, A.R. Miedema, Enthalpies of formation of liquid and solid binary alloys based on 3d metals, Physica B+C 113 (1) (1982) 18–41, https://doi.org/10.1016/0378-4363(82)90107-3. URL, https://linkinghub.elsevier.com/retrieve/pii/0378436382901073.

[96] Q. Guo, O.J. Kleppa, The standard enthalpies of formation of the compounds of early transition metals with late transition metals and with noble metals as determined by Kleppa and co-workers at the University of Chicago — a review, J. Alloys Compd. 321 (2) (2001) 169–182, https://doi.org/10.1016/S0925-8388(01)00956-2. URL, https://linkinghub.elsevier.com/retrieve/pii/S0925838801009562.